JTTEE 3:33-44

A Porosity Formation and Flattening Model of an Impinging Molten Particle in Thermal Spray Coatings

H. Fukanuma

Thermal spray coatings have porosity; however, reasons for the production of porosity during the coating process are not known. This paper proposes a physical and mathematical model for the production of porosity by considering deformation of a molten particle during thermal spray coating processes. The theoretical model shows that the impinging velocity, the ambient gas pressure, the particle diameter, and the molten material viscosity contribute to producing porosity. This paper also proposes that there is a porosity distribution along the splat radius and that most of the porosity exists in the periphery of the splat. Also, a flattening model proposed in this work agrees well with the results of Engel (Ref 1).

1. Introduction

THE boundary structure between splats and the substrate or previously coated layers greatly affects the physical characteristics of thermal spray coatings. In particular, porosity in the thermal spray coating is an important factor in determining the characteristics of the layers. At present, the structures of splat interfaces are being clarified by various studies (Ref 2-6), but there is not yet an established theory of the mechanism of porosity formation in the layers. In this paper, the porosity formation mechanism of thermal spray coatings is mathematically analyzed under several assumptions.

Although there have been some studies concerning the flattening process, they have not theoretically described the flattening process as a function of time (Ref 7, 8). In the present work, a particle flattening model is proposed from a new physical viewpoint. The model includes the radius expansion as a function of time, so that the flattening time can be calculated.

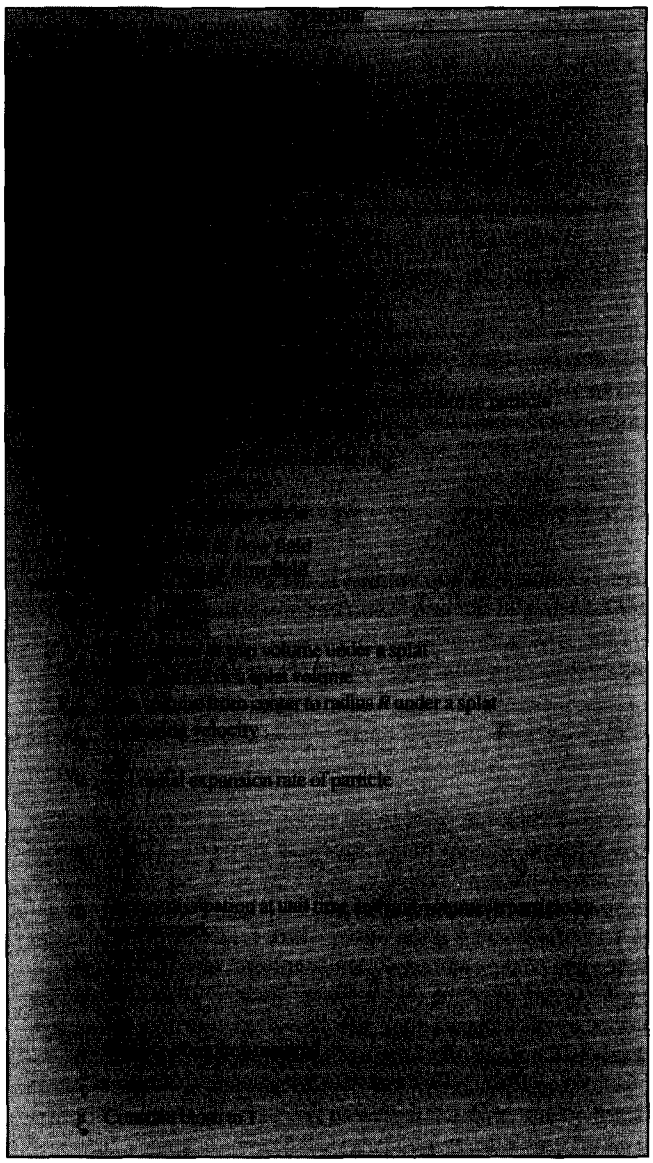

2. Theory

2.1 *Definition of Porosity*

The structure of a thermal spray coating can be pictured as lamellar (Fig. 1), where a first layer of splats is in contact with the substrate. It is known that gaps exist between the substrate and the splats, and between the splats themselves. The schematic of an enlarged interface is shown in Fig. 2. It is assumed that the interface consists of two parts, the gap and the contact region. The true contact region is defined as the interface where chemical bonding exists. It may be a very small proportion of the interface (Ref 3). The contact distance should be at the atomic level such that gas molecules or atoms do not pass through the interfaces. Arata et al. have shown that these gaps are continuous (Ref 5, 6).

Key Words: coating structure, mathematical analysis, numerical model. particle flattening behavior, porosity

H. Fukanuma, Plasma Giken Co., Ltd., 2-4-2 Bijogi-East Toda City, Saitama, Japan.

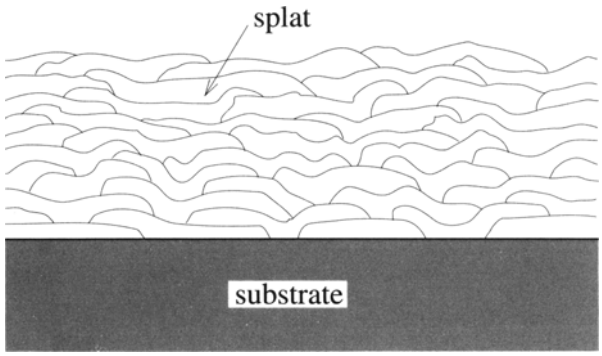

Fig. 1 Schematic of thermal sprayed layers

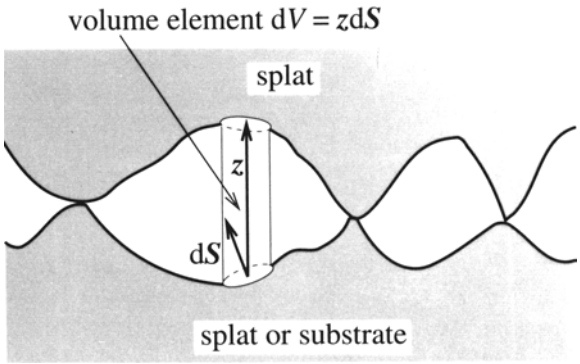

Fig. 2 Schematic of interface between splats or a splat and substrate. The integral of the given zdS element is termed the *gap volume*

These studies suggest that there is little probability that closed pores exist in the interface.

The porosity f_p of the thermal spray coating is defined as:

$$f_p = \frac{V_g}{V_S + V_g} \quad \text{(Eq 1)}$$

where V_g is the total gap volume in the intersplat and splat-substrate interface in the unit volume of thermal spray coating and V_S is the total solid volume in the unit volume of the thermal spray coating. The total gap volume, V_g, is defined as follows:

$$V_g = \frac{1}{2}\int_s z\,dS \quad \text{(Eq 2)}$$

where z is a vector parallel to the z-axis with a length $|z| = z$ (the z-axis is perpendicular to the substrate surface); dS is a vector perpendicular to the small area dS on the splat surface, positive to the outer direction of the splat and with length equal to the surface area of dS; and S is the total surface area of all splats in the unit volume of the coating. V_g is the volume sum of every dV in the splat interface of the unit volume. Since $dV = z\,dS$, V_g can be obtained by the integration of $z\,dS$. However, when integration is carried out for the surface area of every splat, integration is performed twice (i.e., both the lower and upper surfaces of each splat are integrated) and therefore the resultant value is divided by two to calculate the total gap volume.

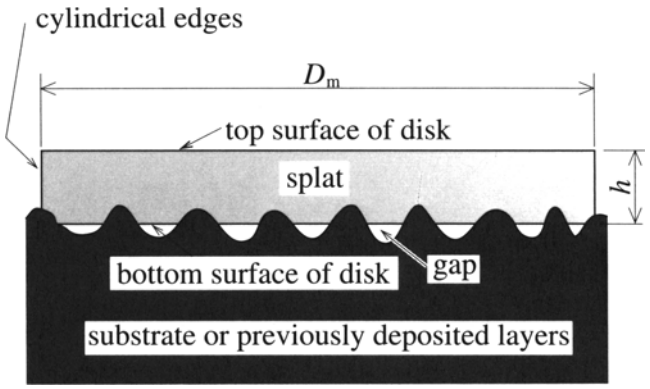

Fig. 3 Schematic of gaps between splat and substrate or previously deposited layers

The "z-distribution" of the interface can describe thermal spray coatings better than porosity. In other words, to know the "z-distribution" is to know the interface structure. Although it is considered to be a more important factor than porosity, it is difficult to measure and analyze theoretically.

It is reasonable to assume that V_S and V_g can be replaced by a splat volume and the gap volume under the splat, respectively, as shown in Fig. 3, because the cylindrical surface area of the splat (i.e., the surface area of the splat edges) is negligible compared to its flat surface area when it is a thin disk. When the diameter and the thickness of the splat are D_m and h, respectively, the two flat surface areas of the top and bottom disks are $2\pi(D_m/2)^2$ and the cylindrical surface area is $\pi D_m h$. The ratio of $\pi D_m h$ to $2\pi(D_m/2)^2$ is expressed as:

$$\frac{\pi D_m h}{2\pi\left(\frac{D_m}{2}\right)^2} = \frac{4}{3}\frac{1}{\left(\frac{D_m}{d_0}\right)^3} \quad \text{(Eq 3)}$$

where d_0 is the diameter of the molten particle at the moment of impingement. Actually, because Eq 3 is a negligibly small value compared to Eq 1, when D_m/d_0 is larger than 3, the cylindrical area is negligible compared to the area of the flat surface. Hereafter, the porosity in the case of a single splat is discussed instead of the unit volume of the thermal sprayed coating.

2.2 *A Mathematical Model of Porosity Formation*

2.2.1 Gas Compression in a Hole by a Rigid Body Impingement

Initially, consider a gas compressed by a moving rigid body. The rigid body plunges into a hole on a substrate at initial velocity v_0 and compresses the gas, as shown in Fig. 4. When the rigid body velocity is reduced to v, the gas pressure is expressed by the polytropic equation

$$P = kV^{-n} \quad \text{(Eq 4)}$$

where P is gas pressure, k is the gas constant, V is gas volume, and n is the polytropic exponent. It is assumed that the gas is ideal, there is no gas leakage through the boundary between the rigid body and the hole wall, and there is no friction between the

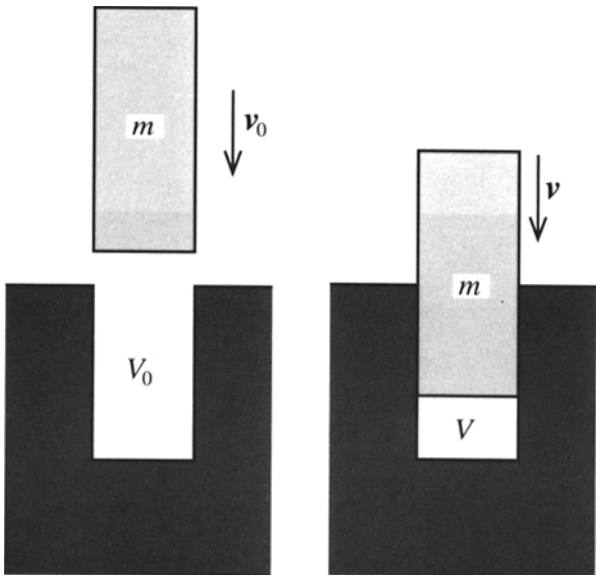

Fig. 4 Schematic of gas compression by a moving rigid body

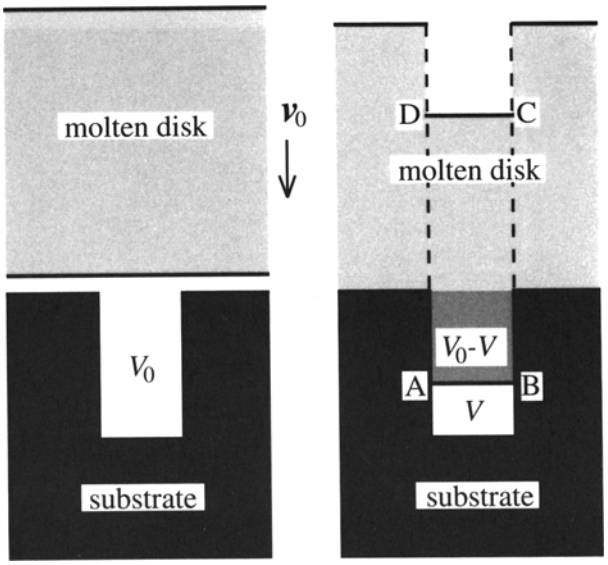

Fig. 5 Schematic of gas compression by a molten disk

body and the wall. In this case, $n = 1$ for isothermal compression, and n is $\gamma = C_P/C_V$ for a reversible adiabatic compression, where C_P and C_V are the specific heat of gas at constant pressure and constant volume, respectively. When the gas volume is compressed to V from V_0 and the velocity of the rigid body is reduced to $\mathbf{v}$ from $\mathbf{v}_0$, under the reversible adiabatic condition, the energy transfer to the gas from the rigid body equals the energy that the rigid body loses. So the next equation holds:

$$\int_{V_0}^{V} -PdV = \int_{V_0}^{V} -kV^{-\gamma}\,dV = \frac{1}{2}m(\mathbf{v}_0^2 - \mathbf{v}^2) \qquad \text{(Eq 5)}$$

where m is the mass of the rigid body.

2.2.2 Gas Compression in a Hole by a Molten Disk

Next, consider the gas compression in the hole by a molten disk impinging on the substrate instead of the rigid body, as shown in Fig. 5. If there is no friction in the molten material and at the interface between the molten material and the wall, and there is no flow parallel to the substrate in the liquid and no gas leakage through the interface, the molten material ABCD compresses the gas in the hole as in the case of the rigid body. Since the mass of ABCD can be replaced by $k_1\rho(V - V_0)$, where k_1 is a constant and ρ is the density of the molten material, the following equation holds:

$$\int_{V_0}^{V} -kV^{-\gamma}dV = \frac{1}{2}k_1\rho(V_0 - V)(\mathbf{v}_0^2 - \mathbf{v}^2) \qquad \text{(Eq 6)}$$

There are other conditions that may affect the gas volume V and must be considered in the case of a molten material compressing the gas:

- Gas leakage through the boundary at the hole wall during the compression process
- Friction between the molten material and the hole wall
- Viscous work in the molten material
- Heat transfer from the liquid to the gas and from the gas to the substrate
- Flow of the molten material parallel to the substrate surface
- The contact angle between the molten material and the substrate or previously coated layers
- The vapor pressure of the molten material (unless this is negligible)

The parameter n can be used in place of γ and represents the difficulty of compressibility. The parameter n is influenced by the above factors and is larger than 1. The molten material stops in the hole when $\mathbf{v} = 0$, and the next equation holds:

$$\int_{V_0}^{V} -kV^{-n}dV = \frac{1}{2}k_1\rho(V_0 - V)\mathbf{v}_0^2 \qquad \text{(Eq 7)}$$

Integrating Eq 7 and substituting $kV_0^{-n} = P_0$ yields the equation:

$$\frac{\left(\frac{V}{V_0}\right)^{1-n} - 1}{1 - \frac{V}{V_0}} = \frac{(n-1)k_1\rho\mathbf{v}_0^2}{2P_0} \qquad \text{(Eq 8)}$$

where P_0 is the gas pressure at gas volume V_0.

When $V/V_0 << 1$, because $1 - V/V_0 \cong 1$ and $(V/V_0)^{1-n} - 1 \cong (V/V_0)^{1-n}$, Eq 8 can be simplified as:

$$\frac{V}{V_0} = \left[\frac{(n-1)k_1\rho\mathbf{v}_0^2}{2P_0}\right]^{1/(1-n)} \qquad \text{(Eq 9)}$$

The ratio of the compressed volume V to the initial volume V_0 decreases as the impinging velocity increases and the ambient pressure decreases; that is, the porosity decreases under these conditions. Figure 6 shows the relationship between the gas

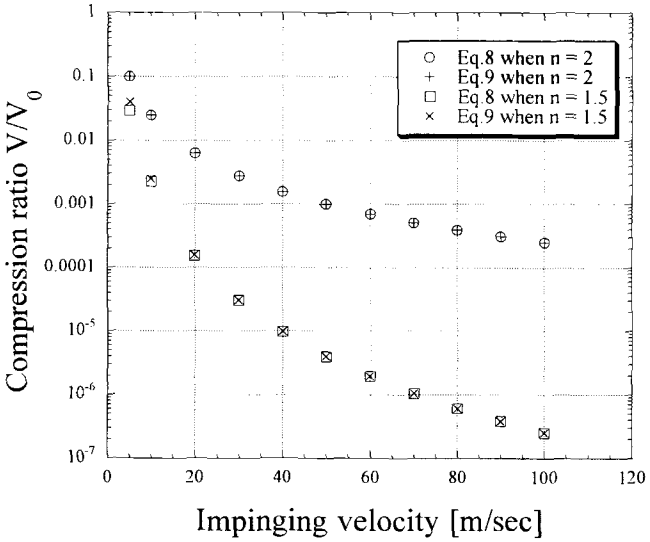

Fig. 6 Relationship between compression ratio and impinging velocity

compression ratio and the impinging velocity in Eq 8 and 9 when $\rho = 8000$ kg/m^3, $P = 10^5$ Pa, $k_1 = 10$, and $n = 1.5$ or 2. It also shows that V/V_0 in Eq 9 agrees with V/V_0 in Eq 8. The expression $k_1 = 10$ means that when the molten disk of 10 μm thickness impinges on the substrate, the molten material enters into the hole to 1 μm depth.

2.2.3 Solidification Time of Molten Material in a Hole

The material is pressed away from the developing gas interface if the molten material does not solidify and the gas pressure is high. If the molten material does solidify in the hole, then the solidification time of the material must be considered. Figure 7 is a schematic of the solidification of molten material. When the temperature of the substrate and the molten material are T_{S0} and T_0, respectively, at time 0, and T_{S0} is held constant and the molten material thickness is semi-infinite, the solidified thickness X at time t is expressed as:

$$X = 2\lambda\sqrt{\kappa_s t} \qquad \text{(Eq 10)}$$

where λ is a numerical constant (detailed in Eq 11), and κ_S and t are the thermal diffusivity of the solidified material and time, respectively (Ref 9). The parameter λ is found from:

$$\frac{\exp(-\lambda^2)}{\text{erf}(\lambda)} - \frac{K_L}{K_S}\frac{\sqrt{\kappa_S}}{\sqrt{\kappa_L}}\frac{(T_0 - T_m)}{(T_m - T_{S0})}\frac{\exp\left(-\frac{\kappa_S}{\kappa_L}\lambda^2\right)}{\text{erfc}\left(\sqrt{\frac{\kappa_S}{\kappa_L}}\lambda\right)} = \frac{\sqrt{\pi}L\lambda}{C_S(T_m - T_{S0})} \qquad \text{(Eq 11)}$$

where K_S and C_S are the thermal conductivity and the specific heat of the solidified material, and K_L, κ_L, T_m, and L are the thermal conductivity, the thermal diffusivity, the melting temperature, and the latent heat of the solidified material, respectively.

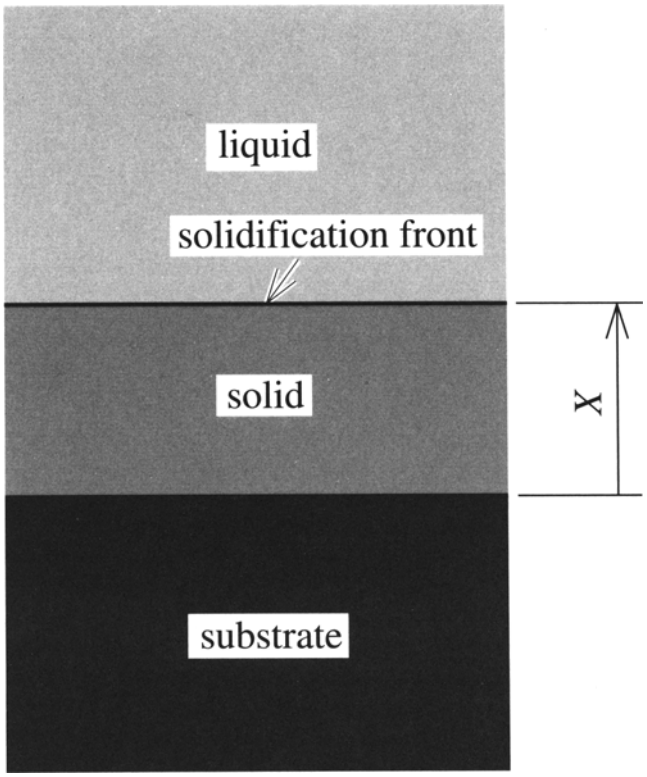

Fig. 7 Schematic of solidification front of molten material

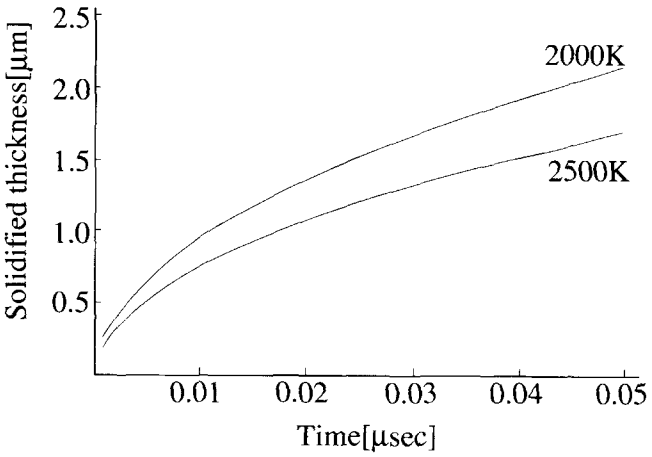

Fig. 8 Relationship of solidified thickness and time for molten copper

Figure 8 shows the results calculated for a copper substrate sprayed with copper particles at 2000 and 2500 K using the physical property values in Table 1. Now, consider a cylindrical hole with a diameter and depth of 1 μm and 1 μ, and assume that the solidification thickness is half of the hole diameter. Because the solidification thickness is 0.5 μm in a 1 μm-diam hole, the solidification time of the molten copper in the hole is about 3×10^{-9} s when the initial temperature of the molten copper is 2000

Table 1 Physical properties of copper

Physical property	Solid copper	Molten copper
Density, Kg/m^3	8780	8780
Specific heat, J/Kg · K	427	495
Heat conductivity, W/m · K	341	180.4
Thermal diffusivity, m/s	9.11×10^{-5}	4.15×10^{-5}
Latent heat, KJ/Kg	205	...
Melting point, K	1357.6	...

K, and about 5×10^{-9} at 2500 K in Fig. 7. When the solidification time is 5×10^{-9} s, the molten copper enters the hole to a depth of 0.5 μm or less at an impinging velocity of 100 m/s, and to a depth of 1 μm or less at an impinging velocity of 200 m/s. The true solidification time is greater than the calculated results because the heat transfer coefficient at the interface between the substrate and the solidified material is far smaller than the assumption used for a thermal spray coating.

Consider a 10 μm thick disk of molten copper compressing gas in the hole (1 μm deep) when the impinging velocity is 200 m/s. Substituting $v_0 = 200$ m/s, $\rho = 8780$ kg/m^3, $P_0 = 1$ atm $= 1.013 \times 10^5$ Pa, $k_1 = 10$, and $n = 2$, $V/V_0 = 5.8 \times 10^{-4}$ is obtained. Because $V/V_0 = 0.58 \times 10^{-5}$, the molten copper almost reaches to the hole bottom. It takes 5×10^{-9} s for molten copper to reach the bottom at speeds of at least 200 m/s. However, because the velocity of the particle is decelerated by the compressed gas in the hole, it takes longer than 5×10^{-9} s for the molten material to reach the bottom. Because solidification begins from the hole wall during the compression process, when the top of the molten material reaches to the hole bottom most material in the hole is solidified. When the hole diameter and depth are of the order of 1 μm or less, it is reasonable to assume that the solidification of the top of the molten material in the hole occurs during the compression process. The remaining high-pressure gas leaks through the boundary, and the pressure equalizes at ambient pressure.

Only one simply shaped hole has been considered for porosity formation with respect to the trapped gas phenomenon. It is reasonable to assume that the hole volume V_0 represents the sum of hole volumes on a unit surface area of the substrate or previously coated layers. The argument also holds when the hole shapes are not cylindrical.

2.3 *A Mathematical Model of Flattening*

Flattening models of liquid droplets that impinge on a rigid flat surface have been proposed (Ref 1, 7, 8), and this paper develops a prior investigation (Ref 10). Because molten particles impinge on a substrate, flatten, and solidify, the particle-gas interaction during flattening must be considered to understand porosity formation.

2.3.1 Radial Expansion Shortly After Impingement

It is assumed that immediately after a molten particle impinges on a flat substrate, a thin radial disk begins to spread, and that the splat thickness is a constant during the flattening, as shown in Fig. 9. The disk spreads under the kinetic energy that is mainly dissipated by viscous work. The disk thickness is probably a function of the impinging velocity, the particle diameter, and the viscosity of the molten material. The assumption agrees with the results of high-speed photographs of a water drop spreading in Engel's investigation (Ref 1). However, in his investigation Engel assumed that the disk thickness at center is half of the peripheral thickness. The following are also assumed:

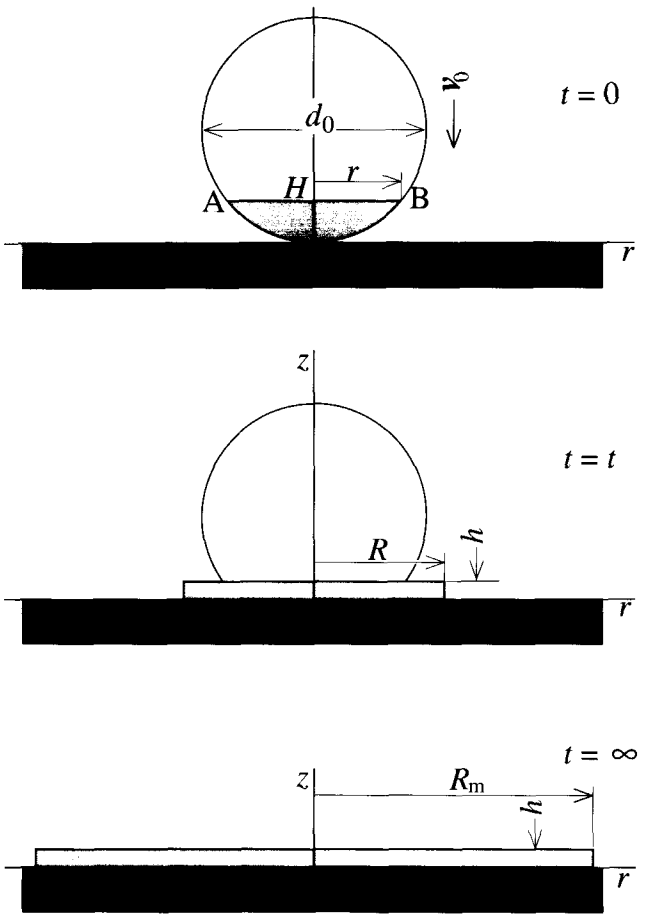

Fig. 9 Schematic of the flattening process

- The flattening process is isothermal (i.e., the viscosity and density of the molten material are constant).
- The kinetic energy that the particle possesses at impingement is dissipated only by viscous friction in the molten material.
- The friction work in the disk only contributes to the energy dissipation, but the friction work in the part of the sphere on the disk can be negligibly small.
- The surface tension of molten material, the interface tension between the material and the substrate, and gravity can also be negligible, as they are generally far less than the kinetic energy experienced during thermal spraying.

Additional assumptions from the present work are:

- The impinging particle is completely molten.

- The particles impinge perpendicularly on the substrate or the previously coated layers, which are smooth.
- Flattening is completed before solidification.
- The particle does not rotate at impingement.
- There is no flow in the particle before impingement.

Consider a molten particle of diameter d_0 that impinges at velocity $\mathbf{v}_0$. At time $t = 0$, a bottom portion of the particle is deformed to a flat disk whose thickness and radius are h and R, respectively. When cylindrical coordinates are used, the volume of 0AB, now identified as ω, is expressed as:

$$\omega = \int_0^H \pi r^2 dz \qquad \text{(Eq 12)}$$

where r is the cord radius made by the sphere of AB length, and H is the height of the bottom portion of the sphere, as shown in Fig. 9. The parameter r can be expressed as:

$$r^2 = \left(\frac{d_0}{2}\right)^2 - \left(\frac{d_0}{2} - z\right)^2 = zd_0 - z^2 \qquad \text{(Eq 13)}$$

Substituting Eq 13 in Eq 12, the expression becomes:

$$\omega = \pi\left(\frac{1}{2}d_0H^2 - \frac{1}{3}H^3\right) \qquad \text{(Eq 14)}$$

When the portion 0AB in the sphere is deformed to the flat disk whose radius and thickness are R and h, respectively, the volume 0AB equals the volume of the disk. Then:

$$\pi hR^2 = \pi\left(\frac{1}{2}d_0H^2 - \frac{1}{3}H^3\right) \qquad \text{(Eq 15)}$$

When $H << d_0$ then:

$$\frac{dH}{dt} = |\mathbf{v}_0| = v_0 \qquad \text{(Eq 16)}$$

Differentiation of Eq 15 by t leads to an expression for the expansion rate of the disk. Because $H = v_0 t$, the expansion rate can be expressed as:

$$\frac{dR}{dt} = \frac{dH}{dt}\sqrt{\frac{d_0}{2h}}\frac{1 - \frac{H}{d_0}}{\sqrt{1 - \frac{2H}{3d_0}}}$$

$$= v_0\sqrt{\frac{d_0}{2h}}\frac{1 - \frac{v_0 t}{d_0}}{\sqrt{1 - \frac{2v_0 t}{3d_0}}} \qquad \text{(Eq 17)}$$

When $H/d_0 << 1$, Eq 17 is simplified as:

$$\frac{dR}{dt} = v_0\sqrt{\frac{d_0}{2h}} \qquad \text{(Eq 18)}$$

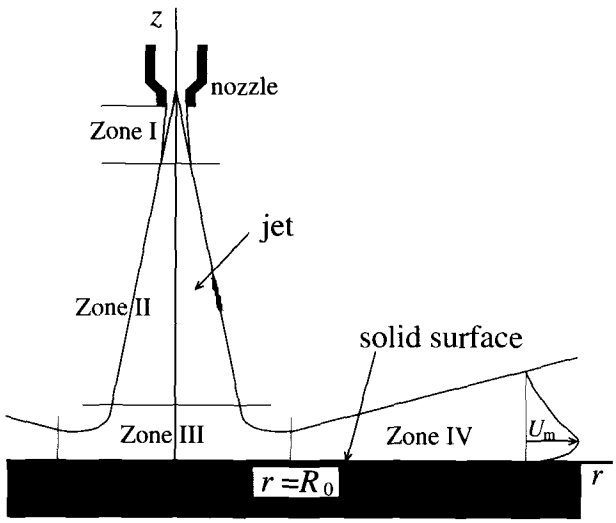

Fig. 10 Schematic of the flow of an impinging jet

Consequently, the radial expanding rate of the disk is obtained shortly after impingement.

2.3.2 The Flow Field in the Disk

Consider a jet impinging on a flat surface as shown in Fig. 10, the flow field consists of four distinct zones. The maximum radial velocity U_m along the r axis is (Ref 11-13):

$$U_m \propto r, \quad r \le R_0 \quad \text{(Zone III)}$$

$$U_m \propto \frac{1}{r}, \quad r > R_0 \quad \text{(Zone IV)} \qquad \text{(Eq 19)}$$

Flow zones III and IV are divided at $r = R_0$. U_m increases proportionally with r and becomes maximum at $r = R_0$, then decreases in inverse proportion to r.

When the flow field in the disk of the impinged particle is defined as $\boldsymbol{u} = \boldsymbol{u}(u_r, u_\theta, u_z)$, then u_r, u_θ, and u_z are the r, θ, and z components of the flow field, respectively, in cylindrical coordinates. From the analogy of impinging jets, it is assumed that the radial velocity u_r is proportional to the radius when $r \le R_0$ and is inversely proportional to the radius when $r > R_0$. The parameter R_0 is a function of the impinging velocity, the particle diameter, and viscosity, and it is assumed that R_0 is close to the radius of the impinging particle ($d_0/2$). Therefore the flow field $\boldsymbol{u} = \boldsymbol{u}(u_r, u_\theta, u_z)$ is:

$$u_r = C_1(t)\, z\,(2h - z)r, \; u_\theta = 0,$$

$$u_z = -\,C_1(t)z^2\left(2h - \frac{2}{3}z\right) \quad \text{for } r < R_0$$

and

$$u_r = C_2(t)\frac{z(2h - z)}{r}, \; u_\theta = 0, \; u_z = 0 \quad \text{for } r \ge R_0 \qquad \text{(Eq 20)}$$

where h is the disk thickness and $C_1(t)$ and $C_2(t)$ are coefficients that are a function of time.

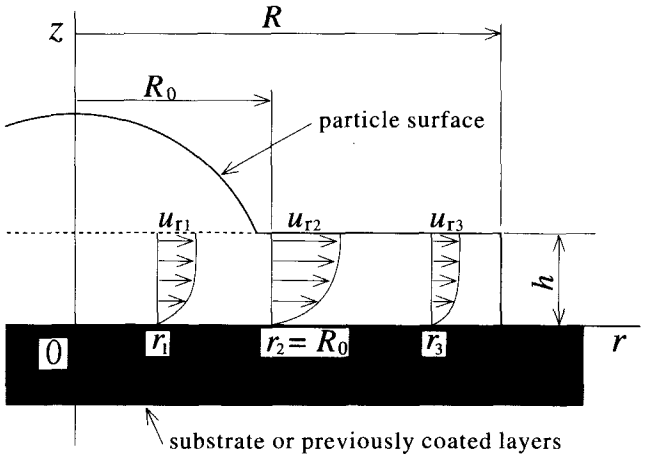

Fig. 11 Schematic of laminar flow in the liquid disk

The flow field must satisfy the equation of continuity, namely div $\boldsymbol{u} = 0$, and meet the following requirements: (a) no shear stress on the free surface; (b) no flow on the substrate surface; and (c) when $r \rightarrow \infty$, $u_r \rightarrow 0$. The flow field $\boldsymbol{u}$ satisfies all of these conditions. The flow field is symmetrical around the z-axis (because no particle rotation at impingement is assumed), so u_θ equals 0.

The flow field could be assumed to be laminar in the disk when the impinging velocity is less than 250 m/s (Fig. 11), because the Reynolds number is substantially below 5000. For example, Reynolds number 5000 occurs when density ρ, the mean radial flow velocity $\bar{u}_r$, representative length h, and viscosity μ are 10^4 kg/m^3, 250 m/s, 2 μm, and 10^{-3} Pa · s, respectively.

Because it is expected that the flow field decreases rapidly with time, then:

$$C_1(t) = C_{10}e^{-\alpha t} \tag{Eq 21}$$

$$C_2(t) = C_{20}e^{-\alpha t} \tag{Eq 22}$$

where C_{10}, C_{20}, and α are constants. There is a volume balance of material about R_0 such that the material that flows from the inside region of R_0 is the same volume that flows into the outside region of R_0. Therefore:

$$\int_0^h C_{10}e^{-\alpha t}z(2h - z)R_0 dz = \int_0^h \frac{C_{20}e^{-\alpha t}z(2h - z)}{R_0} dz \tag{Eq 23}$$

Equation 23 is simplified as:

$$C_{20} = C_{10}R_0^2 \tag{Eq 24}$$

The flow field can be determined when C_{10}, C_{20}, and α are known under certain boundary conditions. For example, when the disk radius becomes R_0 and R at times t_0 and t, respectively, the fluid volume outside R_0 equals the volume that flows out of R_0 for the time from t_0 to t. Hence at the time difference $\tau = t - t_0$:

$$\pi h(R^2 - R_0^2) = 2\pi R_0 \int_0^\tau \int_0^h \frac{C_{20}e^{-\alpha\tau}z(2h - z)}{R_0} dz d\tau \tag{Eq 25}$$

Equation 25 is simplified as:

$$R^2 - R_0^2 = \frac{4C_{20}h^2(1 - e^{-\alpha\tau})}{3\alpha} \tag{Eq 26}$$

When Eq 26 is differentiated and $\tau = 0$ is substituted, then the expression becomes:

$$\left(\frac{dR}{dt}\right)_{\tau=0,R=R_0} = \frac{2C_{20}h^2}{3R_0} \tag{Eq 27}$$

When $\tau = 0$, $t = t_0$, and $R = R_0$, substituting $t = t_0$ in Eq 17, the expression becomes:

$$\left(\frac{dR}{dt}\right)_{t=t_0,R=R_0} = v_0\sqrt{\frac{d_0}{2h}}\frac{1 - \frac{v_0 t_0}{d_0}}{\sqrt{1 - \frac{2v_0 t_0}{3d_0}}} \tag{Eq 28}$$

When $R_0 \leq d_0$, $v_0 t_0/d_0$ is negligible in Eq 28, then:

$$\frac{2C_{20}h^2}{3R_0} = v_0\sqrt{\frac{d_0}{2h}} \tag{Eq 29}$$

Then, C_{20} can be determined as follows:

$$C_{20} = \frac{3R_0 v_0}{2h^2}\sqrt{\frac{d_0}{2h}} \tag{Eq 30}$$

Substituting Eq 30 in Eq 24, the expression becomes:

$$C_{10} = \frac{3v_0}{2h^2 R_0}\sqrt{\frac{d_0}{2h}} \tag{Eq 31}$$

In Eq 26, letting $R = R_m$ when $\tau = \infty$, the expression becomes:

$$\alpha = \frac{2R_0 v_0}{(R_m^2 - R_0^2)}\sqrt{\frac{d_0}{2h}} \tag{Eq 32}$$

Because C_{10}, C_{20}, and α are found above, the flow field is determined.

2.3.3 A Flattening Model

From an energy balance, we find:

$$E_k - \int_0^\infty \dot{\Phi}\, dt - \int_{S_0}^{S_1} \gamma_L\, dS - \int_0^{S_2} \gamma_{SL}\, dS = 0 \tag{Eq 33}$$

where

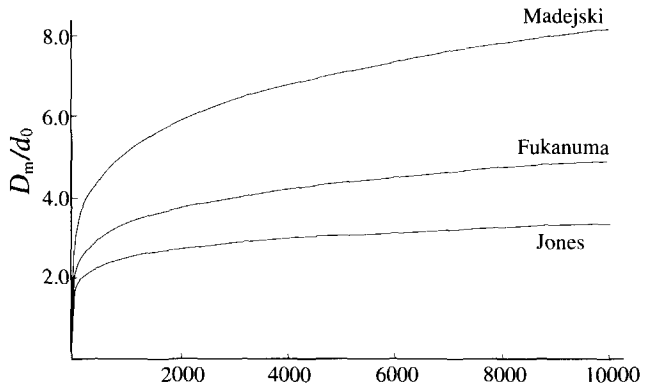

Fig. 12 Relationship between the flattening ratio and Reynolds number

- E_k is the kinetic energy of the particle at the moment of impingement.
- $\int_0^\infty \dot{\Phi} dt$ is the viscous work in the molten material during flattening.
- $\int_{S_0}^{S_1} \gamma_L dS$ is the surface energy that the molten material obtains from surface area S_0 to S_1 during flattening.
- $\int_0^{S_2} \gamma_{SL} dS$ is the interfacial energy obtained by the molten material wetting the area S_2 of the substrate or the coated layers during flattening.
- γ_L and γ_{SL} are the surface tension and the interfacial tension, respectively.
- $\dot{\Phi}$ is the energy that the molten material dissipates by internal friction per unit time during flattening (Ref 14).

From the flow field $\boldsymbol{u}$, because the disk thickness h is thin (i.e., h is negligibly small compared to disk radius R), $\partial u_z/\partial r$ is negligibly small compared to $\partial u_r/\partial z$ and $\dot{\Phi}$ is written as:

$$\dot{\Phi} = \int_V \mu \left(\frac{\partial u_r}{\partial z}\right)^2 dV \qquad \text{(Eq 34)}$$

where μ is the viscosity of molten material and V is the entire volume of molten material. Substituting Eq 20 in Eq 34 and then substituting the result in Eq 33, assuming that the surface and interfacial energy are negligible, the expression becomes:

$$\frac{1}{12}\pi\rho d^3 v_0^2 - \int_0^\infty \int_0^{R_0} \int_0^h \mu \left[\frac{\partial}{\partial z} C_{10} e^{-\alpha t} z(2h - z) r\right]^2 2\pi r dz dr dt$$

$$- \int_0^\infty \int_{R_0}^{R_m} \int_0^h \mu \left[\frac{\partial}{\partial z} \frac{C_{20} e^{-\alpha\tau} z(2h - z)}{r}\right]^2 2\pi r dz dr d\tau = 0 \qquad \text{(Eq 35)}$$

Substituting Eq 30, Eq 31, and Eq 32, and $h = d_0^3/6R_m^2$ in Eq 35, the expression becomes:

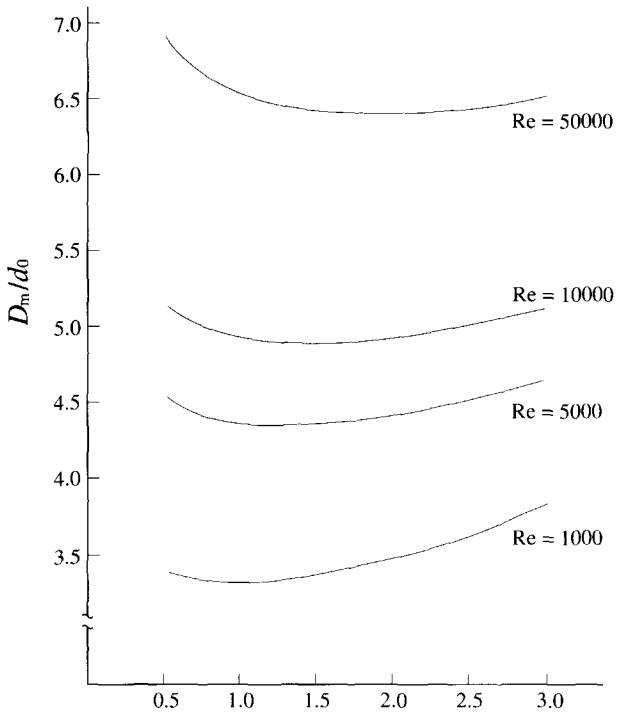

Fig. 13 Relationship between the flattening ratio and the parameter ε

$$\frac{\pi\rho d_0^3 v_0^2}{12} - \frac{9\sqrt{3}\pi\mu v_0 R_0 R_m^7}{d_0^4(R_m^2 - R_0^2)}\left(-\frac{1}{2} + \frac{R_0^2}{2R_m^2} + \ln\frac{R_m}{R_0}\right) = 0 \qquad \text{(Eq 36)}$$

Letting $D_m = 2R_m$, $R_0 = \varepsilon d_0/2$, where ε is in the neighborhood of 1, and substituting them in Eq 36, the expression becomes:

$$\left(\frac{D_m}{d_0}\right)^5 \frac{\varepsilon\left(-\frac{1}{2} + \frac{\varepsilon^2 d_0^2}{2D_m^2} + \ln\frac{D_m}{\varepsilon d_0}\right)}{\left(1 - \frac{\varepsilon^2 d_0^2}{D_m^2}\right)} = \frac{16}{27\sqrt{3}}\frac{\rho d_0 v_0}{\mu} \qquad \text{(Eq 37)}$$

When $\varepsilon = 1$, Eq 37 is approximated as follows:

$$\frac{D_m}{d_0} = 1.06\left(\frac{\rho d_0 v_0}{\mu}\right)^{1/6} \qquad \text{(Eq 38)}$$

When Reynolds number (Re) is $\rho d_0 v_0/\mu$, the expression becomes:

$$\frac{D_m}{d_0} = 1.06\ \mathrm{Re}^{1/6} \qquad \text{(Eq 39)}$$

The disk diameter at $t = \infty$ is determined.

Madejski's theory, Jones' theory, and this theory are shown in Fig. 12, where the flattening ratios as a function of Reynolds number are shown. Madejski's and Jones' theories are, respectively (Ref 8, 9):

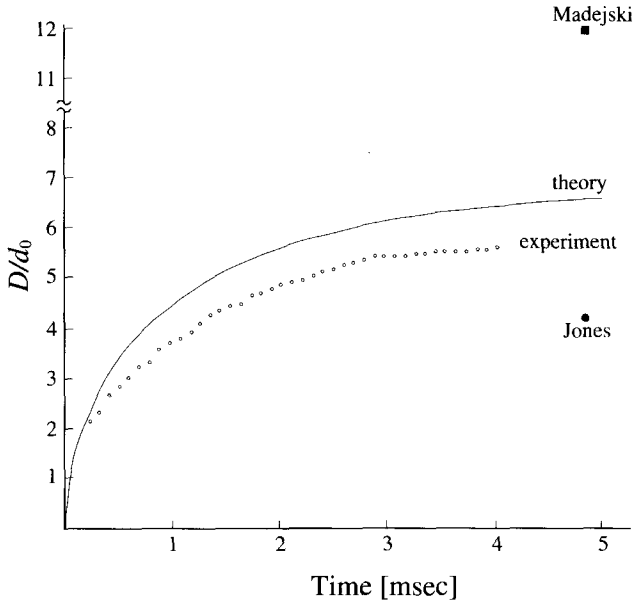

Fig. 14 Engel's experimental results and theoretical results

$$\frac{D}{d_0} = 1.294\ \mathrm{Re}^{1/5} \qquad \text{(Eq 40)}$$

$$\frac{D}{d_0} = 1.059\ \mathrm{Re}^{1/8} \qquad \text{(Eq 41)}$$

In actual flattening process, it is considered that R_0/d_0 must change with time and that therefore ε probably changes from 1 to 2. When the impinging velocity is faster, R_0/d_0 must be larger. However, D_m/d_0 changes little with ε between 1 and 2, as shown in Fig. 13, so ε can be considered a constant.

Substituting Eq 30 and Eq 32 in Eq 26, when $R = D/2$, $R_0 = d_0/2$, and $R_m = D_m/2$, Eq 26 is simplified as:

$$\frac{D}{d_0} = \sqrt{\frac{D_m^2}{d_0^2} - \left(\frac{D_m^2}{d_0^2} - 1\right)\exp\left(\frac{-2\sqrt{3}\frac{D_m}{d_0}\frac{v_0}{d_0}\tau}{\left(\frac{D_m^2}{d_0^2} - 1\right)}\right)} \qquad \text{(Eq 42)}$$

The spreading disk diameter is determined as a function of time. When $1/(D_m/d_0)^2 << 1$, Eq 42 is simplified as:

$$\frac{D}{d_0} = \frac{D_m}{d_0}\sqrt{1 - \exp\left(-2\sqrt{3}\frac{v_0}{d_0}\frac{\tau}{\frac{D_m}{d_0}}\right)} \qquad \text{(Eq 43)}$$

Substituting Eq 39 in Eq 43, the expression becomes:

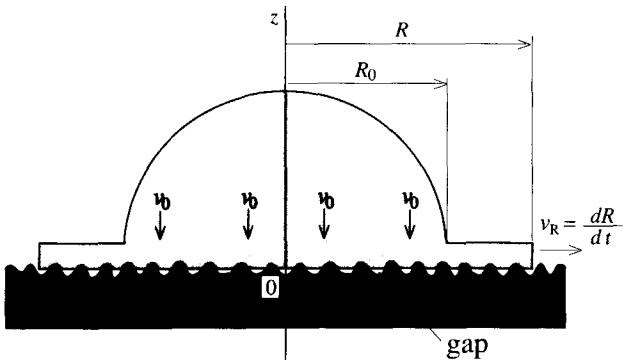

Fig. 15 Schematic of the interaction between molten particle and substrate

$$\frac{D}{d_0} = 1.06\,(\mathrm{Re})^{1/6}\sqrt{1 - \exp\left(-3.67\frac{v_0}{d_0}\frac{\tau}{(\mathrm{Re})^{1/6}}\right)} \qquad \text{(Eq 44)}$$

From Eq 43, the spreading time is determined as:

$$\tau = \frac{1}{2\sqrt{3}}\frac{d_0}{v_0}\frac{D_m}{d_0}\log\left[\frac{1}{1 - \left(\frac{D}{D_m}\right)^2}\right] \qquad \text{(Eq 45)}$$

When $R = R_0$, $t = t_0$. Substituting $H = v_0 t$, $h = 2d_0^3/3D_m^2$, and $R_0 = d_0/2$ in Eq 15, because H/d_0 is negligible, t_0 is determined as follows:

$$t_0 = \frac{1}{\sqrt{3}}\frac{d_0}{v_0}\frac{d_0}{D_m} \qquad \text{(Eq 46)}$$

Because $t = t_0 + \tau$, t is expressed as:

$$t = \frac{1}{2\sqrt{3}}\frac{d_0}{v_0}\frac{D_m}{d_0}\left\{\frac{2d_0^2}{D_m^2} + \log\left[\frac{1}{1 - \left(\frac{D}{D_m}\right)^2}\right]\right\} \qquad \text{(Eq 47)}$$

When the first term in Eq 47 is negligible, t becomes:

$$t = \frac{1}{2\sqrt{3}}\frac{d_0}{v_0}\frac{D_m}{d_0}\log\left[\frac{1}{1 - \left(\frac{D}{D_m}\right)^2}\right] \qquad \text{(Eq 48)}$$

Substituting Eq 39 in Eq 48, the time for the disk to spread to $D = 0.9D_m$ is:

$$t_{0.9} = 0.479\frac{d_0}{v_0}\frac{D_m}{d_0} = 0.508\frac{d_0}{v_0}\mathrm{Re}^{1/6} \qquad \text{(Eq 49)}$$

and the time for the disk to spread to $D = 0.99\ D_m$ is:

$$t_{0.99} = 1.13\frac{d_0}{v_0}\frac{D_m}{d_0} = 1.20\frac{d_0}{v_0}\mathrm{Re}^{1/6} \qquad \text{(Eq 50)}$$

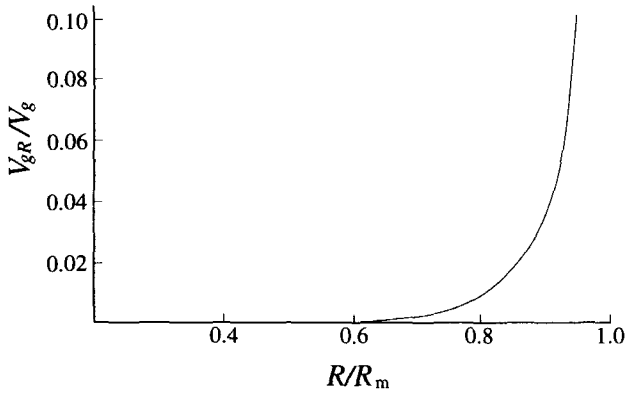

Fig. 16 Relationship between accumulative distribution of gap volume and R/R_m, when $n = 1.5$

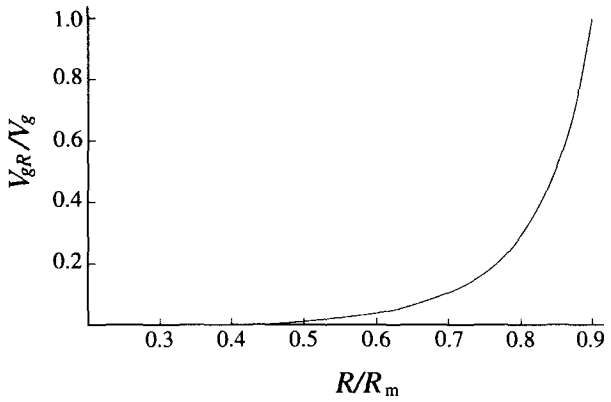

Fig. 17 Relationship between accumulative distribution of gap volume and R/R_m, when $n = 2$

where $t_{0.9}$ and $t_{0.99}$ are the times when the disk diameter becomes $0.9D_m$ and $0.99\,D_m$, respectively. Equations 49 and 50 show that determining the real spreading time is difficult, because the spreading rate is slower in the neighborhood of the maximum diameter. Figure 14 shows that the theory agrees well with the experimental results of Engel (Ref 1) and shows Madejski's and Jones' flattening ratios.

2.4 *Porosity Formation Model with Flattening Process*

The simple theory of porosity formation was described in section 2.2 for the case where a molten disk impinges on a flat substrate having small holes. This section describes a porosity formation model that considers the flattening process. When $V(R)$ is the gap volume per unit area at radius R of the splat, the entire gap volume V_g between the splat and the substrate surface or previously sprayed layers is expressed as:

$$V_g = \int_0^{R_m} V(R) 2\pi R dR \qquad \text{(Eq 51)}$$

It is assumed that the impinging velocity v_0 affects the gas between the splat and substrate surface in the region inside the radius R_0 and that the radial spreading rate $dR/dt = v_R$ affects the gas in the region outside R_0, as shown in Fig. 15. Because Eq 9 is the approximation of Eq 8, when $v_0 \to 0$, $V \to V_0$ in Eq 8. However, $V \to \infty$ in Eq 9. When $R \to R_m$, $v_R \to 0$, so that $V(R) \to \infty$. In order to avoid that, Eq 9 diverges at $R = R_m$, the equation $V(R)$ is substituted for Eq 9, using a parameter ξ that is a numerical value close to and smaller than 1. So $V(R)$ is:

$$V(R) = V_0 \left[\frac{(n-1)k_1 \rho v_0^2}{2P_0}\right]^{1/(1-n)} \qquad 0 \le R < R_0,$$

$$V(R) = V_0 \left[\frac{(n-1)k_1 \rho v_R^2}{2P_0}\right]^{1/(1-n)} \qquad R_0 \le R < \xi R_m,$$

$$V(R) = V_0 \qquad \xi R_m \le R \le R_m \qquad \text{(Eq 52)}$$

Substituting Eq 52 in Eq 51, the expression becomes:

$$V_g = \int_0^{R_0} V_0 \left[\frac{(n-1)k_1 \rho v_0^2}{2P_0}\right]^{1/(1-n)} 2\pi R dR$$

$$+ \int_{R_0}^{\xi R_m} V_0 \left[\frac{(n-1)k_1 \rho v_R^2}{2P_0}\right]^{1/(1-n)} 2\pi R dR$$

$$+ \int_{\xi R_m}^{R_m} V_0 2\pi R dR \qquad \text{(Eq 53)}$$

The radial spreading rate v_R can be determined by substituting Eq 30 and Eq 32 after differentiating Eq 26 with respect to time as follows:

$$v_R = \frac{dR}{dt} = \frac{\sqrt{3} R_m v_0}{2(R_m^2 - R_0^2)} \frac{R_m^2 - R^2}{R} \qquad \text{(Ref 54)}$$

The gap volume V_{gR} from $R = 0$ to R is defined as:

$$V_{gR} = \int_0^R V(R) 2\pi R dR \qquad \text{(Eq 55)}$$

The accumulative distribution of gap volume V_{gR}/V_g is determined by integrating Eq 53 and Eq 55, after substituting Eq 54 in Eq 53 and Eq 52 in Eq 55 because the values in $0 \le R < R_0$ of Eq 53 and Eq 55 are negligible compared with those in $R_0 \le R \le R_m$. Also, when R_0^2 / R_m^2 is negligible, the expressions become, respectively,

$$\frac{V_{gR}}{V_g} = \frac{\left(\frac{R}{R_m}\right)^6}{\left(1 - \frac{R^2}{R_m^2}\right)^3} \frac{(1-\xi^2)^3}{\xi^6} \quad \text{for } n = 1.5 \qquad \text{(Eq 56)}$$

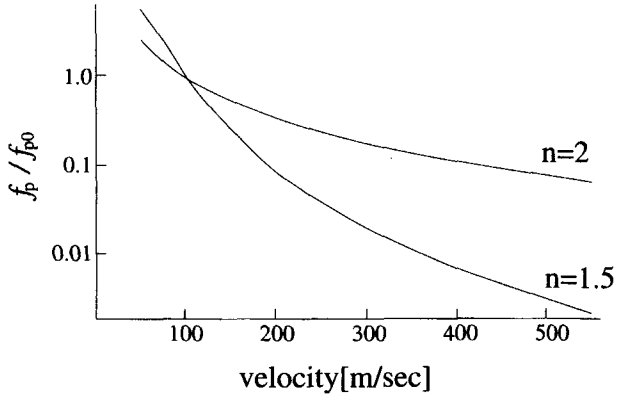

Fig. 18 Relationship between porosity and impinging velocity as f_{p0} = 0.1 at 100 m/s and n = 1.5 and 2

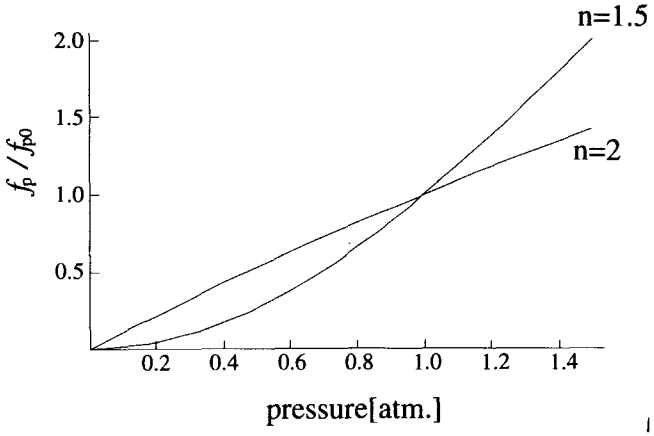

Fig. 19 Relationship between porosity and ambient pressure as f_{p0} = 0.1 at 1 atm and n = 1.5 and 2

$$\frac{V_{gR}}{V_g} = \frac{\left[\dfrac{\dfrac{R^2}{R_m^2}}{\left(1-\dfrac{R^2}{R_m^2}\right)} + \log\left(1-\dfrac{R^2}{R_m^2}\right)\right]}{\left[\dfrac{\xi^2}{(1-\xi^2)} + \log(1-\xi^2)\right]} \quad \text{for } n = 2 \qquad \text{(Eq 57)}$$

Figures 16 and 17 show V_{gR}/V_g as a function of the normalized radius R/R_m, when n = 1.5 and n = 2. They show that the gap volume increases with increasing radius and becomes extremely large in the periphery of the splat. Figure 16 shows that when n = 1.5, most gap volume exists outside $0.9R_m$ (i.e., in the peripheral region of the splat). When n = 2, the gap volume begins to increase from about 0.4 R_m; it becomes about 10% up to approximately 0.7 R_m. It is shown that most gap volume exists in the periphery of the splat.

Porosity is defined by Eq 1. When same-size molten particles impinge at different velocities and all other conditions are the same, then the ratio at impinging velocity v_0 to the porosity at v_{00} is expressed as:

$$\frac{f_p}{f_{p0}} = \frac{\dfrac{V_g}{V_S + V_g}}{\dfrac{V_{g0}}{V_S + V_{g0}}} = \frac{V_g}{V_{g0}} \frac{1}{1 + \left(\dfrac{V_g}{V_{g0}} - 1\right) f_{p0}} \qquad \text{(Eq 58)}$$

where V_g and V_{g0} are the gap volumes at impinging velocities v_0 and v_{00}, respectively; f_p and f_{p0} are the porosities at v_0 and v_{00}, respectively. V_S is a splat volume; and V_g for $0 \le R < \xi R_m$ is simplified in Eq 59 and 60. It is assumed that R_0^2/R_m^2 and the first term on the right-hand side of Eq 53 and are negligible, therefore, integrating the second term, the expression becomes:

$$V_g = 1.06^2 \frac{4}{27}\pi V_0 \left(\frac{4P_0}{k_2\rho}\right)^2 \left(\frac{\rho d_0}{\mu}\right)^{1/3} \frac{1}{v_0^{11/3}} \left[\frac{\xi^6}{(1-\xi^2)^3}\right]$$

for n = 1.5 (Eq 59)

$$V_g = 1.06^2 \frac{1}{3}\pi V_0 d_0^2 \left(\frac{2P_0}{k_2\rho}\right) \left(\frac{\rho d_0}{\mu}\right)^{1/3} \frac{1}{v_0^{5/3}} \left[\frac{\xi^2}{(1-\xi^2)} + \log(1-\xi^2)\right]$$

for n = 2 (Eq 60)

The porosity ratio is shown as a function of impinging velocity in Fig. 18 as f_{p0} = 0.1 at 100 m/s and n = 1 and 2. Figure 19 shows the porosity ratio as a function of ambient pressure as f_{p0} = 0.1 at 1 atm. Figures 18 and 19 show that porosity decreases with increasing impinging velocity and increases with increasing ambient pressure. Equations 59 and 60 show that porosity decreases as the density or viscosity of the molten material increases. These results seem to be confirmed by empirical knowledge.

3. Conclusion

According to the theory developed in this article, the gap volume between the splat and the substrate or previously coated layers is minimal in the central portion and relatively larger in the periphery of the splat. It is believed that the interaction force between the splat and the substrate within the radius R_0 is very different from that outside it, because the flow field $\boldsymbol{u}$ outside R_0 shows that pressure is zero on the substrate surface. The pressure at the impingement point is $a\rho C_0 v_0$ at the moment of impingement (Ref 1), where a is a constant (about 0.5) and C_0 is the velocity of a compression wave in the molten particle. This gradually becomes smaller as the flattening particle expands to R_0. The bonding force inside R_0 is probably stronger than that outside R_0. Interaction between the molten particle and the substrate is strongly affected by the impinging velocity inside R_0, but not that outside R_0. Although wettability of coating material onto the substrate or of coating material onto prior solidified material is not directly considered in this theory, it might influence the interface interaction very much outside R_0. This would be particularly true in the periphery of the splat, when the molten material wets the substrate. The radial spreading rate is as fast as the impinging velocity in the neighborhood of R_0, so it is questionable whether the rate at which molten material wets the sub-

strate is faster than the spreading rate and whether the wetting action contributes to the interaction when the spreading rate is fast. However, because the spreading rate is slow in the outer part of the splat, wettability becomes important for porosity and bonding. It is believed that the velocity affects porosity and bonding when $r < R_0$ and that the wettability is of prime concern when $r > R_0$.

This theory illustrates that gaps must be continuous. It is believed that closed pores are not produced in the flattening process, because it is difficult for molten material to seal the hole completely against the high pressure. Gas probably escapes from the hole opening somewhere in the interface between the molten material and the substrate. Many paths for gas to escape through the interface are made during flattening. With the same reasoning, there are few true contact areas in the interface on the atomic level, and thus the bonding force is produced by an anchor effect or mechanical bond in thermal spray coating. If the molten particle temperature is sufficient to melt the substrate material, or if the substrate temperature is so high that it is molten, closed pores could conceivably be produced as molten particles impinge, and metal or chemical bonding may be achieved.

REFERENCES

1. O.G. Engel, Waterdrop Collisions With Solid Surfaces, *J. Res. Nat. Bur. Stand.*, Vol 54 (No. 5), May 1955, p 281-298
2. R. McPherson, The Relationship Between the Mechanism of Formation, Microstructure, and Properties of Plasma Sprayed Coatings, *Thin Solid Films*, Vol 83, 1981, p 297-310
3. R. McPherson and B.V. Shafer, Interlamellar Contact Within Plasma-Sprayed Coatings, *Thin Solid Films*, Vol 97, 1982, p 201-204
4. S. Safai and H. Herman, Microstructural Investigation of Plasma-Sprayed Coatings, *Thin Solid Films*, Vol 45, 1977, p 295-307
5. Y. Arata, A. Ohmori, and C. Li, Electrochemical Method to Evaluate the Connected Porosity in Ceramic Coatings, *Thin Solid Films*, Vol 156, 1988, p 315-325
6. Y. Arata, A. Ohmori, and C. Li, Study on the Structure of Plasma Sprayed Ceramic Coating by Using Copper Electroplating, *Proc. ATTC* (Osaka, Japan), May 1988, p 205-210
7. H. Jones, Cooling, Freezing and Substrate Impact of Droplets Formed by Rotary Atomization, *J. Appl. Phys.*, Vol 4, 1971, p 1657-1660
8. J. Madejski, Solidification Droplets on a Cold Surface, *Int. J. Heat Transfer*, Vol 19, 1976, p 1009-1013
9. H.S. Carlow and J.C. Jaeger, *Conduction of Heat in Solids*, 2nd ed., Oxford University Press, Oxford, England, 1959, p 285
10. H. Fukanuma, An Analysis of the Porosity Producing Mechanism, *Thermal Spray: International Advances in Coatings Technology*, C.C. Berndt, Ed., ASM International, 1992, p 767-772
11. N. Rajaratnam, Chapter 11, *Turbulent Jets*, Elsevier Scientific Publishing Co., 1981 (translated to Japanese)
12. M. Poreh and J.E. Cermark, Flow Characteristics of a Circular Submerged Jet Impinging Normally on a Smooth Boundary, *Proc. Sixth Mid-Western Conf. on Fluid Mechanics*, 1967, p 198-212
13. S. Beltaos and N. Rajaratnam, Impinging Circular Turbulent Jet, *Proc. A.S.C.E. J. Hydraulics Division*, 1974, p 1313-1328
14. L.D. Landau and E.M. Lifshitz, *Fluid Mechanics*, 2nd ed., Pergamon Press, Oxford, England, 1987, p 50-51